Supporting Information

Ryan et al. 10.1073/pnas.0905654106

SI Materials and Methods

Lipid Extraction and TLC Analyses. Tissue and cell pellets were weighed and placed in 1 mL ice-cold methanol acidified with 2% acetic acid and extracted as described in ref. 1. For LC-ESI-MS, a 46-μL sample, consisting of 10 μL lipid extract, 5 μL deuterated standards (2.5 ng/species), and 31 μL 0.1% formic acid in H_2O, was analyzed per MS run exactly as described in ref. 2. To control for extraction efficiency, human samples were spiked with 187.5 ng C13:0 LPC at time of extraction. Where relative estimation is indicated, concentrations were determined in comparison to 1.25 ng d_4-C16:0 PAF or d_4-C_{16}-*lyso*-PAF spiked at the time of MS analysis. Tissue wet weight in grams was divided by the specific gravity of brain tissue (1.050) to obtain the volume in milliliters for molar calculations (3). For TLC, lipid extraction from media and of acid-labile and acid-resistant fractions was performed as described in ref. 1. Briefly, hNTs, terminally differentiated for 6 weeks as described in ref. 4 and seeded at a final density of 1×10^7 cells/10-cm dish, were incubated at 37 °C with 1 μM B-PAF in DMEM/F12 media containing 0.025% BSA for 0, 2, 5, 15, 30, or 60 min. At each time point, four plates/condition were removed from the incubator and placed on ice. Media was removed, and 1 mL ice-cold methanol acidified with 2% acetic acid was added to this extracellular fraction. Cells were washed with 200 mM Na acetate, pH 4.5, 25 mM NaCl, 1% BSA to remove B-PAF present at the plasma membrane or bound to cell surface proteins. This acid-labile fraction was collected and extracted. The remaining monolayer of cells was collected in 1 mL acidified methanol by scraping the plate with a cell lifter (Fisher) representing the intracellular fraction resistant to the 200 mM Na acetate, pH 4.5, 25 mM NaCl, 1% BSA. Lipids were extracted from all three fractions at each time point by the Bligh and Dyer method, developed on TLC plates (20 × 20 cm Silica Gel 60; Fisher) in a solvent system of chloroform/methanol/acetic acid/water (50:30:8:5, vol/vol) using B-PAF and B-*lyso*-PAF (Molecular Probes) as authentic markers. Fluorescent lipids were visualized under UV light using AlphaImager-1220 software (Alpha Innotech). Fluorescence intensity corresponding to lipid yield was determined by densitometry using the Advanced Measurement Module of OpenLab version 3.5 expressed as the percentage of total lipids. Live-cell imaging following exposure to 1 μM C11:0 B-PAF was performed as described in ref. 1.

Neuronal Culture, Treatment, Death, mRNA Analyses, Transfections, and Protein Assays. Cells were treated for up to 24 h with C16:0 PAF (0.01–1 μM), C16:0 lyso-PAF (1 μM), mc-PAF (0.01–5 μM) all from Biomol Research Laboratories, or Aβ_{42} (25 μM; Sigma) prepared as soluble oligomers (5). All treatments were performed in serum-free media containing 0.025% BSA devoid of PAF-AHs (Fig. S8*a*). Some cultures were pretreated for 15 min with roscovitine (0.1–5 μM; Sigma) or vehicle (0.1% DMSO). Treatments were carried out for up to 24 h as indicated. Caspase activity in live cells was measured using CaspaTag (caspase 3/7; Chemicon) or FLICA (caspase 2; Intergen) assays according to the manufacturers' protocol. Cdk5 activity was determined as described in ref. 6. To assess caspase dependence, hNTs were treated with C16:0 PAF (1 μM) or vehicle in the presence and absence of the caspase 2 inhibitor Z-VDVAD-FMK (50 μM) or 3/7 inhibitor Z-DEVD-FMK (50 μM). Cell survival was assessed by LIVE/DEAD Viability/Cytotoxicity assay (Molecular Probes) or TUNEL (Roche). To test functional impact, hNTs were treated with C16:0 PAF (1 μM) in the presence or absence of the caspase 2 inhibitor Z-VDVAD-FMK (50 μM) or the caspase 3/7 inhibitor Z-DEVD-FMK (50 μM) for 24 h. Data were expressed as percent survival relative to vehicle-treated cells. PAF-AH I α_2 in pcDNA 3.1 (kindly provided by Dr. H. Arai, University of Tokyo), or PAF-AH II cloned in our laboratory into pcDNA 3.1 (1) were cotransfected into hNT cells with EGFP in pcDNA3.1 (Invitrogen) by calcium phosphate transfection. Cell survival in serum-free media following C16:0 PAF (1 μM) or Aβ_{42} (25 μM) treatment was calculated as described in ref. 7. Where transfection of PAF-AH II or PAF-AH α_2 with EGFP or empty vector and EGFP is indicated, all treatments were carried out 72 h after transfection when maximal EGFP was observed. Transfection efficiency ($\approx$22%) was comparable in all conditions as established by counting EGFP-positive cells immediately before treatment in each experiment as well as, in separate experiments, PAF-AH II immunoreactive cells. Cell survival was calculated as the EGFP-positive cell number following treatment/mean EGFP-positive cell number in the vehicle control times 100. Data were analyzed by Student's *t* test or ANOVA followed by post-hoc Dunnett's *t* tests or Tukey tests as applicable using Instat v3.0.

Antibodies Used. Western blot analysis was performed using antibodies raised against α_1, α_2, or PAF-AH II (1:1,000; Dr. H. Arai, University of Tokyo), GAPDH (1:2,000; IMGENEX), LIS1 clone 210 (1:5,000; Dr. O. Reiner, Weizmann Institute of Science), BIP/GRP78 (1:1,000; Cell Signaling), αII-spectrum (1:1,000; Sigma), *m*-calpain (1:500; Sigma), tau (AT8, 1:1,000; Sigma), β-tubulin (1:10,000; Sigma), Cdk5 (C-8, 1:1,000; Santa Cruz), p35 (C-19, 1:500; Santa Cruz), p39 (C-20, 1:500; Santa Cruz), phospho-GSK3β (Ser-9, 1:1,000; Cell Signaling), AKT (1:1,000; Cell Signaling), and phospho-AKT (Thr-308, 1:1,000). Secondary antibodies were horseradish peroxidase-conjugated anti-mouse IgG (1:2,000), anti-rabbit IgG (1:5,000), and anti-goat IgG (1:800; all from Jackson Immunolabs) visualized using SuperSignal West Pico (MJS BioLynx). Quantification of protein expression was performed by densitometric analysis of individual bands using ImageJ analysis software [v1.42; National Institutes of Health (NIH)].

Ratiometric Determination of Intracellular Calcium Mobilization. Briefly, hNT neurons on glass coverslips were loaded with 10 μM fura-2-AM plus 0.02% pluronic F-127 (Molecular Probes) for 30 min at 37 °C. After rinsing with PSS Mg^{2+}-free buffer containing 2 mM HEPES, pH 7.2, 140 mM NaCl, 5 mM KCl, 2.3 mM CaCl$_2$, and 10 mM glucose cells were allowed 5 min in the same buffer to stabilize. Coverslips were placed in a microperfusion system housed on the stage of an LSM-410 Zeiss (Carl Zeiss) inverted laser scanning microscope equipped with an argon-krypton ion laser and with a Fluor 40×/0.75W acroplan objective. After a region of interest was chosen, fura-2 fluorescence was measured at 510 nm emission with 340/380 nm dual excitation. The basal level of calcium was recorded for 120 s, followed by the application of the control PSS buffer, supplemented with 0.025% BSA (vehicle) for another 240 s. C16:0 PAF (1 μM) was then applied for 180 s in control buffer followed by a subsequent 60-s wash out with control buffer alone. C16:0 lyso-PAF (1 μM) in control buffer was then applied for 180 s followed again by a 60-s wash out with control buffer alone. Finally, K$^+$ (10 mM) was applied as a positive control and the recording was continued for another 160 s. The 340–380 nm fluorescence ratio (R340/380) for five cells was measured on five independent coverslips.

1. Bonin F, et al. (2004) Anti-apoptotic actions of the platelet activating factor acetylhydrolase I alpha 2 catalytic subunit. *J Biol Chem* 279:52425–52436.

2. Whitehead SN, et al. (2007) Rapid identification and quantitation of changes in the platelet activating factor family of glycerophospholipids over the course of neuronal differentiation by high performance liquid chromatography electrospray ionization tandem mass spectrometry. *Anal Chem* 79:8359–8548.

3. Nelson SR, Mantz ML, Maxwell JA (1971) Use of specific gravity in the measurement of cerebral edema. *J Appl Physiol* 30:268–271.

4. Boucher S, Bennett SA (2003) Differential connexin expression, gap junction intercellular coupling, and hemichannel formation in NT2/D1 human neural progenitors and terminally differentiated hNT neurons. *J Neurosci Res* 72:393–404.

5. Klein WL (2002) Abeta toxicity in Alzheimer's disease: Globular oligomers (ADDLs) as new vaccine and drug targets. *Neurochem Int* 41:345–352.

6. Smith PD, et al. (2003) Cyclin-dependent kinase 5 is a mediator of dopaminergic neuron loss in a mouse model of Parkinson's disease. *Proc Natl Acad Sci USA* 100:13650–13655.

7. Ryan SD, et al. (2007) Platelet activating factor-induced neuronal apoptosis is initiated independently of its G-protein coupled PAF receptor and is inhibited by the benzoate orsellinic acid. *J Neurochem* 103:88–97.

Fig. S1. The alkylacylglycerophosphocholine remodeling pathway (Lands' cycle). Alkylacylglycerophosphocholines can be remodeled to PAFs through the actions of cPLA$_2$ releasing arachidonic acid and LPCAT1 and LPCAT2 with acetyl-CoA as the acyl donor (blue). Individual PAF isoforms are defined by the length and degree of unsaturation of the long chain fatty acid at the *sn*-1 position. PAFs are themselves remodeled back to structural membrane lipids by the actions of any one of three PAF-AH isoforms followed by LPCAT1 or LPCAT2 using acyl-CoA donors (red). In brain, PAF-AH I is neuron-specific. PAF-AH II has additional transacetylase activity that can transfer the free acetyl group to the *sn*-2 position of LPCs and sphingosines. Abbreviations: AAGPC, 1-O-alkyl-2-arachidonoyl-glycerophosphocholine; cPLA$_2$, cytosolic phospholipase A$_2$; LPC, *lyso*phosphatidylcholine; LPCAT, LPC-acyltransferase; PAF, platelet activating factor; PAF-AH, PAF acetylhydrolase.
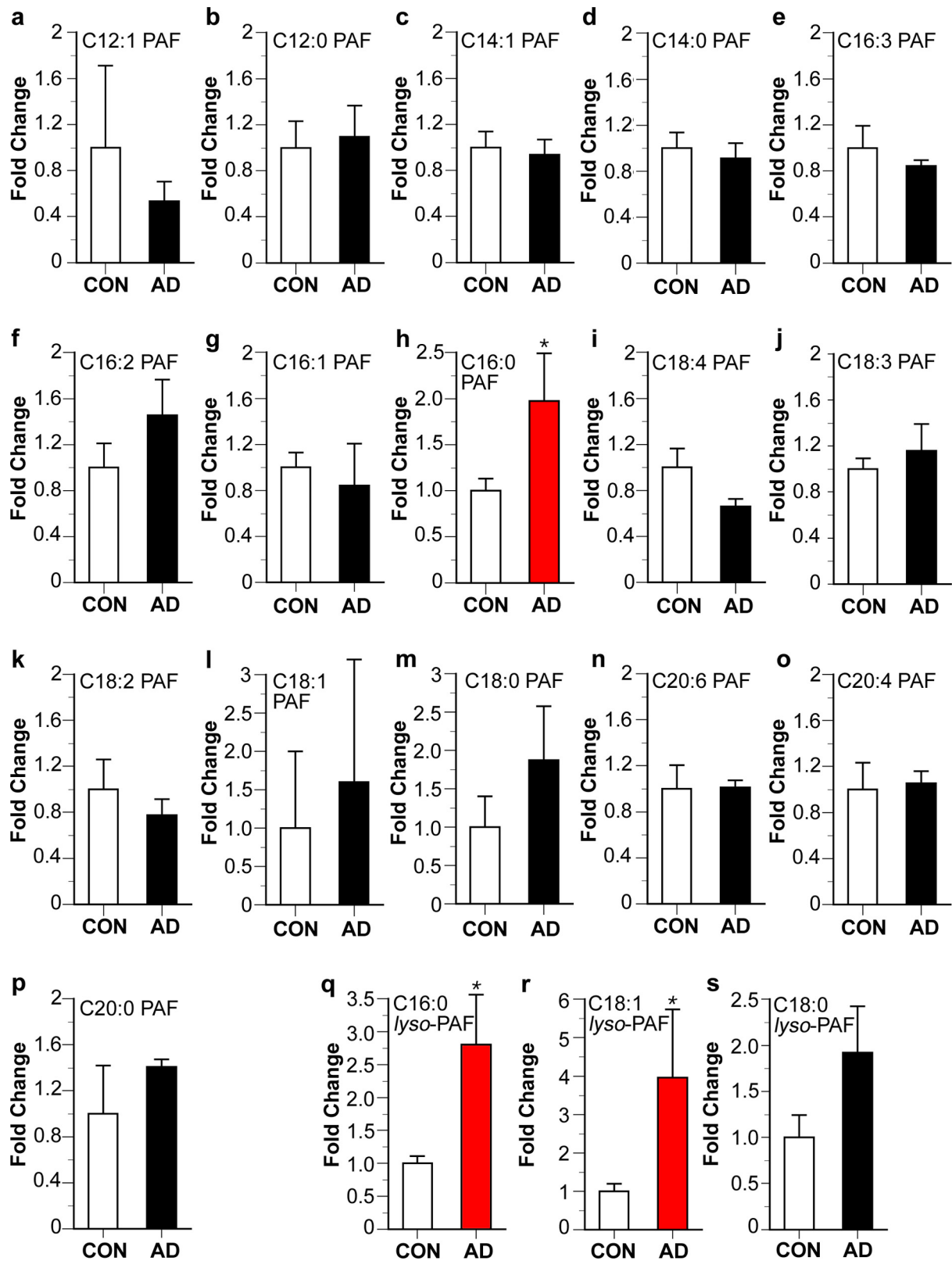
Fig. S2. Specific PAF metabolites accumulate in AD tissue. (*a–p*) Sixteen PAF species and (*q–s*) three *lyso*-PAF species were detected in human posterior/entorhinal cortex by LC-ESI-MS. Predicted structures are indicated in Fig. S3. Species were identified on the basis of mass and retention time. Significant changes in (*h*) C16:0 PAF, (*q*) C16:0 *lyso*-PAF, and (*r*) C18:1 *lyso*-PAF levels were detected in AD tissue (*n* = 4 individuals/condition). Data are expressed as fold change relative to controls + SEM (*, *P* < 0.05, Student's *t* test).
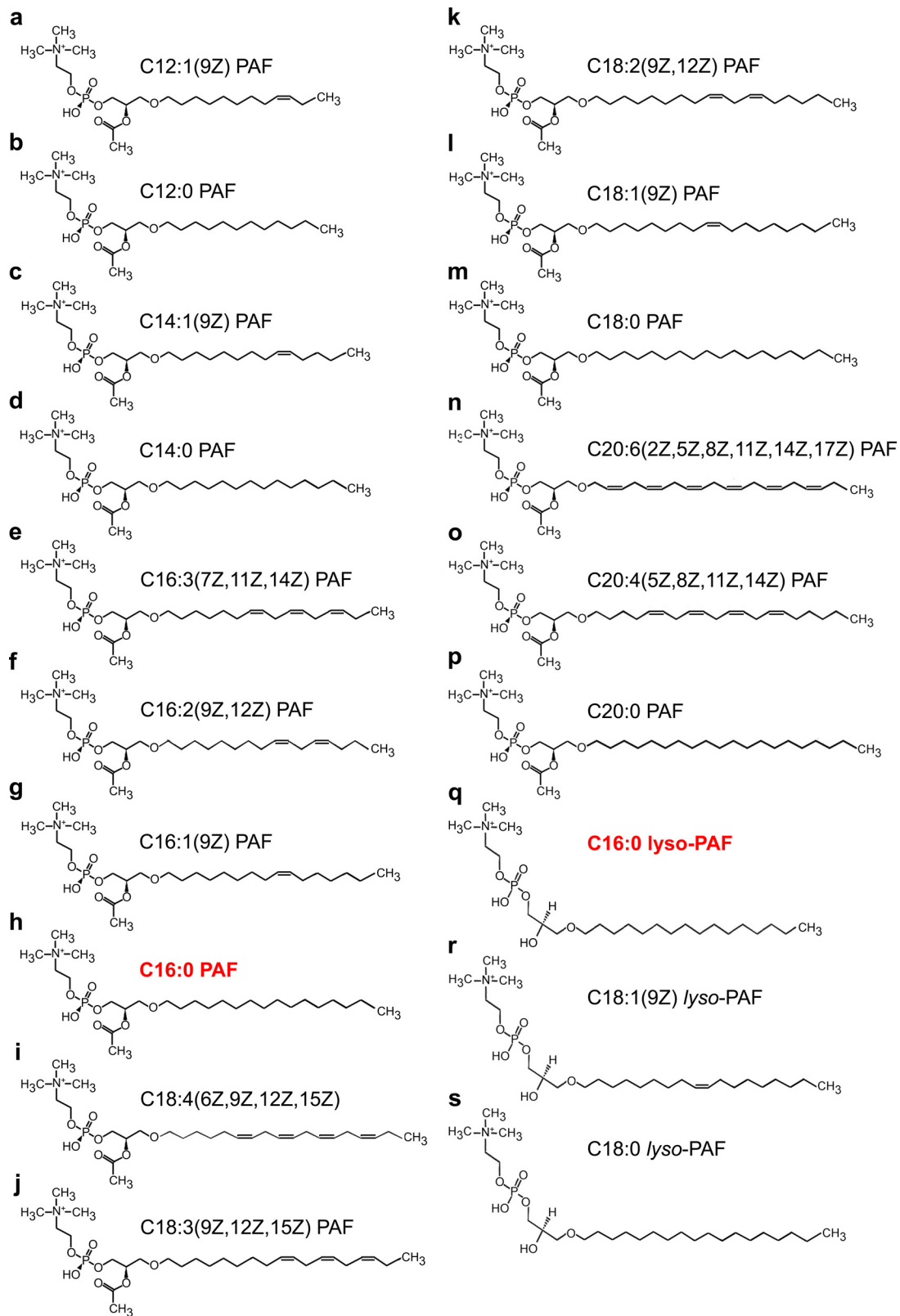
Fig. S3. Predicted PAF structures identified in control and AD cortex. (*a–p*) The predicted structures of the 16 (*a–r*) PAF species and (*q–s*) three *lyso*-PAF species detected in human posterior/entorhinal cortex by LC-ESI-MS with the likely position of double bonds are indicated.
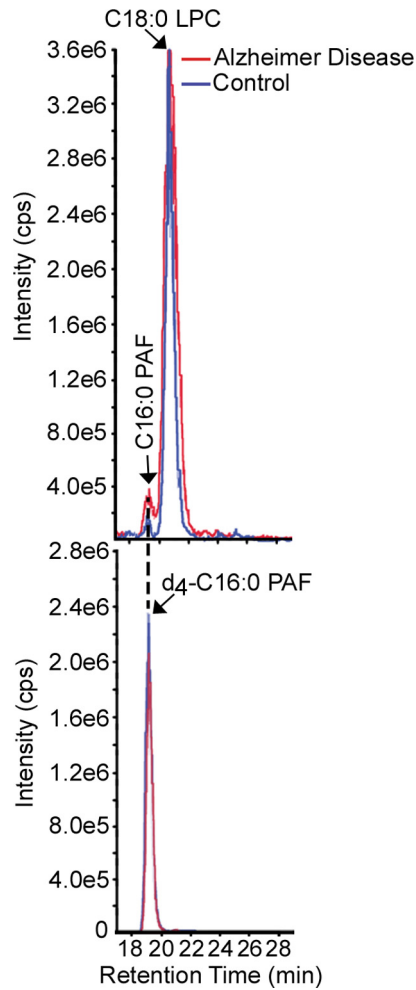
Fig. S4. The identities of C16:0 PAF and C16:0 *lyso*-PAF were verified by co-elution with deuterated standards. As PAF species can be isobaric with other phosphatidylcholines, analytes were reanalyzed following spike with deuterated d4-C16:0 PAF or d4-C16:0 *lyso*-PAF. Representative extracted ion chromatographs at *m/z* 524 (*Upper*) or 528 (*Lower*) with a phosphocholine product ion at *m/z* 184.0 detected by precursor ion scan in positive ion mode are presented. C16:0 PAF clearly separates from isobaric C18:0 LPC (*Upper Inset*) and coelutes with d4-C16:0 PAF (*Lower Inset*).
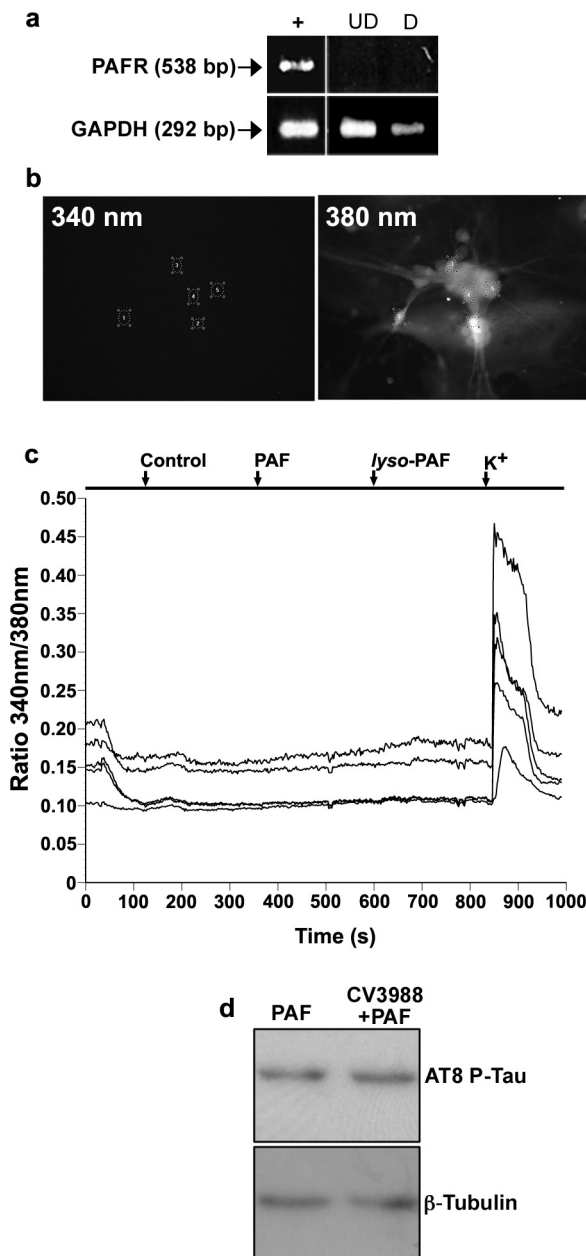
Fig. S5. C16:0 PAF and C16:0 *lyso*-PAF do not elicit signals associated with PAFR activation in PAFR-negative human neurons. (*a*) Undifferentiated NT2/D1 precursor cells (UD) and terminally differentiated hNT neurons (D) do not express PAFR mRNA as determined by RT-PCR. PC12 cells stably transfected with human PAFR(+) were used as a positive control. GADPH was amplified from the same random-primed cDNA to confirm template integrity. (*b*) C16:0 PAF and C16:0-*lyso*-PAF do not acutely mobilize calcium. Fluorescent micrographs depict hNT neurons loaded with the calcium-sensitive indicator Fura-2 AM. Neurons on which quantification was performed are identified numerically as 1–5. *Left* depicts cells during the period of C16:0 PAF exposure. *Right* depicts cells following application of K$^+$ (10 mM) (*C*) Fura-2 fluorescence was measured at 510 nm emission with 340/380 nm dual excitation. The basal level of calcium was recorded for 120 s, followed by the application of the control PSS buffer, supplemented with 0.025% BSA (vehicle) for another 240 s. C16:0 PAF, C16:0 *lyso*-PAF, and finally K$^+$ was then sequentially applied for 180 s in control buffer followed by a subsequent 60-s wash out with control buffer alone. The 340/380 nm fluorescence ratio (R340/380) for five cells was measured on five independent coverslips. Of 25 cells stimulated with C16:0 PAF over five different experiments, none exhibited a calcium response. All of these neurons stimulated with K$^+$ exhibited a robust response. A representative experiment of five replicates is depicted. (*c*) Treatment with 10 μM CV3988, a PAFR-specific antagonist, did not inhibit C16:0 PAF-mediated AT8-reactive tau phosphorylation.

Fig. S6. Internalization and metabolic fate of C11:0 B-PAF and C11:0 B-*lyso*-PAF administered to hNT neurons. (*a*) The kinetics of B-PAF internalization were assessed by live-cell imaging. hNT neurons were incubated with 1 μM B-PAF at 37 °C for 0, 5, 30, 45, 60, and 180 min in serum-free treatment media containing 0.025% BSA. At each time point, B-PAF-containing media were removed and set aside. Cells were washed with PBS plus 1% BSA to remove phospholipids loosely bound to the extracellular face of the plasma membrane, imaged, and the B-PAF-containing media replaced. Data are reported as the mean increase ± SEM in fluorescence intensity standardized to background autofluorescence before treatment. Cell-associated fluorescence increased over the first 60 min of exposure. (Scale bar, 50 μm.) (*b*) The fate of internalized B-PAF was determined by TLC. hNT neurons were treated with 1 μM B-PAF. After 0, 1, 5, 15, 30, and 60 min of exposure, lipids were extracted from three fractions: Extracellular (media), membrane-associated, acid-labile (lipids loosely bound to the plasma membrane), and internalized, acid-resistant (lipids extracted from hNT neurons). Fractions were separated by TLC and species identified in comparison to labeled standards run concurrently. Data represent the relative fluorescence present in each fraction expressed as a percentage of the total labeled lipid recovered and are the mean + SEM of two independent experiments conducted in replicate. C11:0 B-PAF was rapidly internalized by hNT neurons and hydrolyzed to C11:0 B-*lyso*-PAF. The labeled metabolite was released into the extracellular media. Elevated intracellular levels of C11:0 B-PAF remained constant for the first 30 min, dropping gradually once the rate of hydrolysis exceeded the rate of internalization. (*c*) C11:0 B-*lyso*-PAF was also rapidly internalized. Extracellular C11:0 B-PAF associated with the plasma membrane and was internalized within 1 min of exposure. Intracellular lipid was, however, converted to C11:0 B-alkylacylglycerophospho-cholines (C11:0 B-GPC) and not C11:0 B-PAF in the absence of any other toxic stimuli.

Fig. S7. Treatment of hNT neurons with Aβ_{42} induces conversion of internalized C11:0 B-*lyso*-PAF to C11:0 B-PAF. The acid-resistant fractions representing internalized lipid in hNT neurons were analyzed by TLC. In control cultures (−), all of the internalized C11:0 B-*lyso*-PAF was converted to C11:0 B-alkylacylglycerophosphocholine (GPC) (*a*) or released as C11:0 B-*lyso*-PAF (acid-labile fraction; Fig. S6c). In cultures treated with Aβ_{42} (+), more internalized lipid was retained (*c*) and was converted to C11:0 B-PAF (*b*) as compared to C11:0 GPC (*a*).
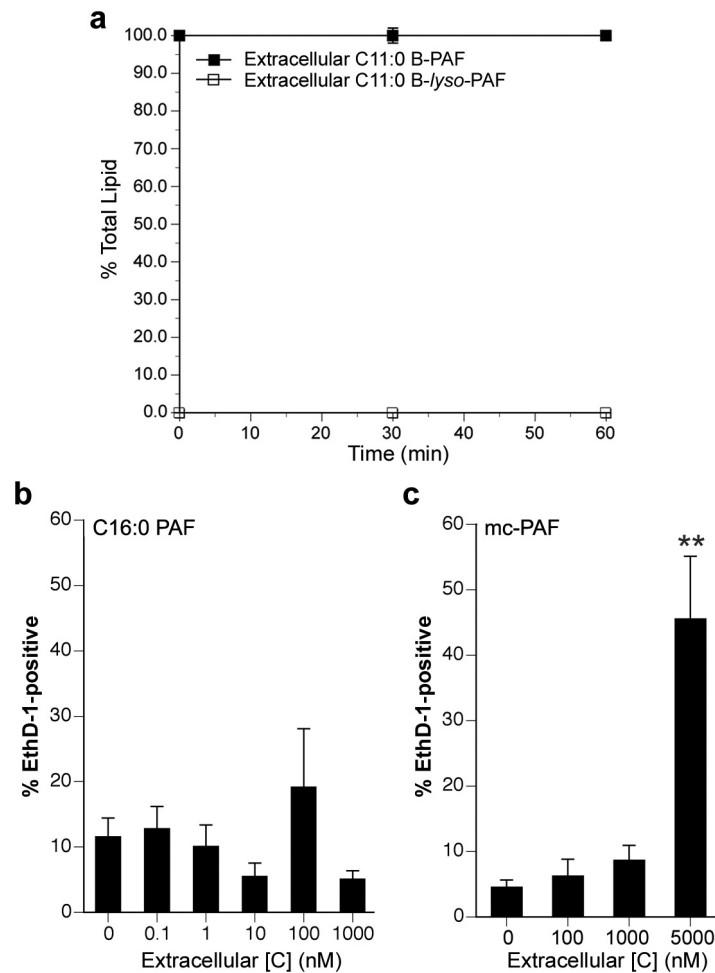
Fig. S8. Direct exposure of hNT neurons in treatment media to C16:0 PAF does not compromise plasma membrane integrity at submicellar concentrations. (*a*) The absence of PAF-AH activity in serum-free treatment media containing 0.025% BSA was confirmed by the addition of a BODIPY fluorophore-labeled C11:0 PAF isoform [1-(O-[11-(4,4-difluoro-5,7-dimethyl-4-bora-3a,4a-diaza-s-indacene-3-proprionyl)amino]undecyl)-2-acetyl-sn-glycero-3-phosphocholine] directly to media with extraction and analysis by TLC. No degradation of C11:0 B-PAF to C11:0 B-*lyso*-PAF was detected when lipids were incubated for up to 60 min at 37 °C in treatment media. (*b*) C16:0 PAF did not cause EthD-1 uptake compared to vehicle-treated control cultures indicating membrane integrity was not impaired. (*c*) Loss of membrane integrity was only observed when PAF hydrolysis was suppressed and extracellular PAF lipid concentrations exceeded critical micelle concentration demonstrated using the PAF-AH-resistant PAF analog mc-PAF.